Acta Pharmacologica Sinica

www.nature.com/aps

ARTICLE

6-Methyl flavone inhibits Nogo-B expression and improves high fructose diet-induced liver injury in mice

Ke Gong[1], Zhen Zhang[1], Sha-sha Chen[1], Xin-ran Zhu[1], Meng-yao Wang[1], Xin-yue Yang[2], Chen Ding[2], Ji-hong Han[1,3], Qing-shan Li[1]✉ and Ya-jun Duan[2]✉

Excessive fructose consumption increases hepatic de novo lipogenesis, resulting in cellular stress, inflammation and liver injury. Nogo-B is a resident protein of the endoplasmic reticulum that regulates its structure and function. Hepatic Nogo-B is a key protein in glycolipid metabolism, and inhibition of Nogo-B has protective effects against metabolic syndrome, thus small molecules that inhibit Nogo-B have therapeutic benefits for glycolipid metabolism disorders. In this study we tested 14 flavones/isoflavones in hepatocytes using dual luciferase reporter system based on the Nogo-B transcriptional response system, and found that 6-methyl flavone (6-MF) exerted the strongest inhibition on Nogo-B expression in hepatocytes with an IC_{50} value of 15.85 μM. Administration of 6-MF (50 mg· kg^{-1} ·d^{-1}, i.g. for 3 weeks) significantly improved insulin resistance along with ameliorated liver injury and hypertriglyceridemia in high fructose diet-fed mice. In HepG2 cells cultured in a media containing an FA-fructose mixture, 6-MF (15 μM) significantly inhibited lipid synthesis, oxidative stress and inflammatory responses. Furthermore, we revealed that 6-MF inhibited Nogo-B/ChREBP-mediated fatty acid synthesis and reduced lipid accumulation in hepatocytes by restoring cellular autophagy and promoting fatty acid oxidation via the AMPKα-mTOR pathway. Thus, 6-MF may serve as a potential Nogo-B inhibitor to treat metabolic syndrome caused by glycolipid metabolism dysregulation.

Keywords: metabolic syndrome; glycolipid metabolism; liver injury; high fructose; 6-methyl flavone; Nogo-B

Acta Pharmacologica Sinica (2023) 0:1–14; https://doi.org/10.1038/s41401-023-01121-7

INTRODUCTION

Fructose, an isomer of glucose, is a common monosaccharide that is able to bind to glucose to form sucrose. High fructose corn sirup (HFCS) is a sugar additive made from fructose and sucrose, accounting for the majority of fructose in daily intake. However, a series of metabolic diseases such as obesity, diabetes, and non-alcoholic fatty liver disease (NAFLD) caused by excessive consumption of HFCS has raised concern worldwide [1–3]. Unlike glucose, fructose does not stimulate insulin and leptin production. Moreover, due to the higher sweetness and palatability of HFCS, excessive consumption occurs more easily, leading to increased obesity. Fructose is absorbed in the small intestine by glucose transporter type 5 and diffuses into intestinal capillaries and is transported to the liver via the portal vein [4]. Unlike glucose, fructose can bypass the rate-limiting glycolytic step mediated by phosphofructokinase. In the absence of hormonal regulation, fructose catabolism occurs without restriction in the liver via ketohexose kinase (KHK) [5]. Carbohydrate-responsive element binding protein (ChREBP) is hyperactivated by a high fructose load compared to glucose to promote hepatic de novo lipogenesis (DNL) more potently and induce metabolic diseases [6]. Therefore, fructose has higher hepatotoxicity than glucose, and this effect is largely based on insulin resistance, oxidative stress, and inflammatory responses due to fructose-induced DNL [7].

Reticulon 4 (Nogo) is a member of the reticulon family and is composed of three primary isoforms, Nogo-A, B, and C. The Nogo-B protein is expressed in various tissues including the liver, blood vessels, heart, kidney, and nervous system [8, 9]. As a protein resident of the endoplasmic reticulum (ER), Nogo-B is pivotal for the regulation of the structure and function of the ER. Additionally, the results of various studies indicate that Nogo-B may be the only member of the Nogo family found in both hepatic parenchymal cells and circulation [10]. Nogo-B is involved in various pathophysiological processes in the liver, including hepatic fibrosis, and cirrhosis [10], hepatocyte proliferation and regeneration [11], alcoholic fatty liver [12], NAFLD-induced hepatocellular carcinoma [13], and cholestasis [14]. Our study has recently revealed that Nogo-B is involved in hepatic glucolipid metabolic processes through the regulation of the ChREBP and insulin pathways. Reducing Nogo-B expression can reduce inflammation, apoptosis, and endoplasmic reticulum stress induced by a high fructose diet (HFrD), thereby effectively inhibiting metabolic disorder development [15]. Accordingly, we hypothesize that Nogo-B has the potential to intervene in the treatment of metabolic syndrome

[1]Key Laboratory of Metabolism and Regulation for Major Diseases of Anhui Higher Education Institutes, Hefei University of Technology, Hefei 230031, China; [2]Department of Cardiology, the First Affiliated Hospital of USTC, Division of Life Sciences and Medicine, University of Science and Technology of China, Hefei 230001, China and [3]College of Life Sciences, State Key Laboratory of Medicinal Chemical Biology, Key Laboratory of Bioactive Materials of Ministry of Education, Nankai University, Tianjin 300071, China
Correspondence: Qing-shan Li (liqs@hfut.edu.cn) or Ya-jun Duan (yajunduan@ustc.edu.cn)
These authors contributed equally: Ke Gong, Zhen Zhang

Received: 2 March 2023 Accepted: 1 June 2023
Published online: 04 July 2023

induced by HFrD and can be a novel target for the design and screening of related drugs.

While no drugs are approved for the treatment of NAFLD, several potential drugs may be used to treat fructose-induced NAFLD [16]. KHK inhibitors have been shown to improve fructose-induced metabolic disorders in rats. In addition, some natural products and plant extracts (e.g., curcumin, resveratrol, and (-)-epicatechin) have received increasing interest. These products can improve excessive DNL, mitochondrial dysfunction, inflammation, and insulin resistance in animal models which were administered an HFrD [17]. Flavonoids are present in plants, and several studies have reported the medicinal value of different flavonoids for cardiovascular disease, liver injury, cancer, and other diseases [18].

Considering Nogo-B as a potential target for the treatment of high fructose-induced metabolic disorders, as well as the general biological activity and therapeutic properties of flavonoids, in this study, we constructed a plasmid including the promoter for Nogo-B to screen 14 flavonoids in hepatocytes and found potential flavonoids that may significantly inhibit hepatic Nogo-B expression. We investigated the therapeutic effect and molecular mechanisms of the flavonoid on HFrD-induced liver injury in mice.

MATERIALS AND METHODS

Reagents

Rabbit anti-NgBR (Cat# ab168351) polyclonal antibody was purchased from Abcam Biotechnology Inc (Cambridge, UK). Rabbit anti-Nogo-B (Cat# NB100-56681) polyclonal antibody was purchased from Novus (USA). Rabbit anti-Lamin A/C (Cat# A0249), FASN (Cat# A0461), SOD1 (Cat# A0274), SOD2 (Cat# A1340), IL-1β (Cat# A16288), TNFα (Cat# A0277), β-actin (Cat# AC026), β-Tubulin (Cat# AC008) polyclonal antibodies were purchased from ABclonal Technology (Woburn, MA, USA). Rabbit anti-CPT1α (Cat# TD12004), Beclin1 (Cat# T55092), LC3B (Cat# T55992), P62 (Cat# T55546), pmTOR (Cat# T56571), mTOR (Cat# T55306), pAMPKα (Cat# T55608), AMPKα (Cat# T55326), CREB (Cat# T55426) polyclonal antibodies were purchased from Abmart (Shanghai, China). Rabbit anti-pNFκB (Cat# AF2006), NF-κB (Cat# AF5006) polyclonal antibodies were purchased from Affinity Biosciences (Cincinnati, USA). Rabbit anti-ACC (Cat# 4190S), pIRS1 (Cat# 2385), IRS1 (Cat# 2382) polyclonal antibodies were purchased from Cell Signaling Technology (USA). Rabbit anti-HSP90 (Cat# 13171-1-AP), ChREBP (Cat# 13256-1-AP), pAKT (Cat# 10176-2-AP), AKT (Cat# 66444-1-Ig) polyclonal antibodies were purchased from Proteintech (Philly, USA).

The AdPlus-mCherry-GFP-LC3B (Cat# C3012) and dihydroethidium (DHE) (Cat# S0063) were purchased from Beyotime Biotechnology (Shanghai, China). The dorsomorphin (Compound C) (Cat# HY-13418A) and DC-CPin7 (Cat# HY-147869) were purchased from MedChemExpress (Jiangsu, China). The Sodium Carboxy-methylcellulose (CMC-Na) (Cat# 419281), Oil red O (Cat# O9755), Palmitic acid (Cat# P0500), and Oleic acid (Cat# O1008) were purchased from Sigma-Aldrich (St Louis, USA). The thiazolyl blue tetrazolium bromide (MTT) (Cat# M8180), glucose (Cat# G8150), insulin (Cat# I8830), D-Fructose (Cat# F8100), and Nile Red (Cat# N8440) were purchased from Solarbio (Beijin, China). The mouse Nogo-B (Cat# RX203233M), IL-1β (RXSWSXB203063M), TNF-α (RXSWSXB202412M) ELISA kit and human TNF-α (RXSWSXB8100010H) ELISA kit were purchased from Ruixin Biological Technology (Quanzhou, China).

Cell culture

HepG2 and Huh7 cells (both human hepatocellular carcinoma cell lines) were all cultured in complete high glucose DMEM medium. The medium contained 10% (vol/vol) fetal bovine serum, 50 μg/mL penicillin/streptomycin. Cells were switched to serum-free medium and received treatment when the confluence was 70%–80%.

According to the mechanism of fructose-induced liver injury [19, 20], cells were co-treated with fatty acids (FA, palmitic acid/oleic acid = 2/1) and fructose to construct the cellular model of liver injury in vitro. The optimal modeling concentration (500 μM FA, 100 mM fructose) was determined by treating cells with a concentration gradient of FA-fructose mixture for 24 h. Subsequently, the effects of 6-methyl flavone (6-MF) as well as the underlying mechanisms were investigated in vitro by the optimized cellular model.

Screening flavonoids by dual luciferase reporter system

All flavonoids were purchased from Titan (Shanghai, China). According to the basic flavonoid structure containing two benzene rings with phenolic hydroxyl groups, we selected the simplest flavones and isoflavones, including those with the same substituent (methyl, methoxy, hydroxyl) at different positions of 5, 6, and 7, and different substituents at the same position. For isoflavones, the primary different substituents were arranged on the C ring. The structures of the specific 14 flavonoids are presented in Table 1. All flavonoids were dissolved in dimethyl sulfoxide. Cells were treated with flavonoids at 10 μM for 24 h, based on the concentration of flavonoids employed in the literature [21, 22].

The pGL4.10 vector (encoding the luciferase reporter gene) containing the human Nogo-B promoter (from −410 to −127) was constructed in a previous study [23] and named H-pNogo-B. HepG2 cells were seeded in 48-well plates at ~90% confluence, followed by transfection of the pGL4.10 vector or H-pNogo-B and *Renilla* luciferase (for internal normalization, pGL4.70), respectively. After treatment with flavonoids, the activity of promoters was determined using a microplate reader (Synergy H1, BioTek, Winooski, USA).

Analysis of cell viability by MTT assay

The MTT assay was used to detect the effect of flavonoids on cell viability. Briefly, HepG2 cells were seeded in 96-well plates with ~10^4 cells per well and treated with flavonoids. After treatment, the medium was replaced with 100 μL medium dissolved with MTT (0.5 mg/mL) and incubated for 4 h at 37 °C. After incubation, the culture solution was replaced with 150 μL of dimethyl sulfoxide and shaken at low speed for 10 min on a shaker to dissolve the crystals. The absorbance of each well was measured at *OD* 490 nm. Cell viability was expressed as fold changes in absorbance compared to the control group.

In vivo studies

All animal experiments were conducted in compliance with the ARRIVE guidelines, and performed following the "*Guide for the Care and Use of Laboratory Animals (the Guide)*" from the National Institute of Health (NIH Publications No. 8023, revised 1978). These experiments were approved by the Ethics Committee of the Hefei University of Technology (HFUT20210601001). C57BL/6J male mice (~8 weeks old at a weight of ~22 g) were purchased from Gempharmatech (Nanjing, China) and housed at 23 ± 1 °C with a relative humidity of 60%–70% under a 12-h/12-h light/dark cycle. All mice had access to water and food *ad libitum*.

Mice were randomly divided into four groups (6 mice per group): group 1 (NC-C), mice were fed normal chow and treated with 200 μL of 0.5% sodium carboxymethylcellulose (CMC-Na) (i.g) per day; group 2 (NC-F), mice were fed normal chow and treated with 6-MF (50 $mg \cdot kg^{-1} \cdot d^{-1}$, the dose selected was based on relevant literature [24, 25]) dissolved in 200 μL of 0.5% CMC-Na (i.g); group 3 (HFrD-C), mice were fed a 70% high fructose diet (HFrD), and treated with 200 μL of 0.5% CMC-Na (i.g) per day; group 4 (HFrD-F), mice were fed HFrD and treated with 6-MF (50 $mg \cdot kg^{-1} \cdot d^{-1}$) in 200 μL of 0.5% CMC-Na (i.g). Throughout the experiment, the body weight, food intake, and appearance of the mice were recorded. We performed glucose (GTT) and insulin (ITT)

Table 1. Structure of the different flavonoids (FL).

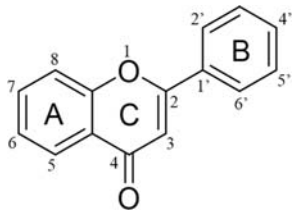

Compd.	5	6	7	4′
FL_1	**OH**	-	-	-
FL_2	-	**OH**	-	-
FL_3	-	-	**OH**	-
FL_4	**OCH_3**	-	-	-
FL_5	-	**OCH_3**	-	-
FL_6	-	-	**OCH_3**	-
FL_7	-	**CH_3**	-	-
FL_8	-	-	**CH_3**	-

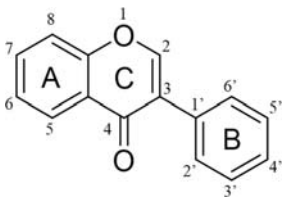

Compd.	5	6	7	4′
FL_9	-	-	**$OCH(CH_3)_2$**	-
FL_10	-	-	**OH**	**OCH_3**
FL_11	-	**OCH_3**	**OCH_3**	**OCH_3**
FL_12	-	-	**OH**	**OH**
FL_13	-	-	**OH**	**OCH_3**
FL_14	**OH**	-	**OH**	**OCH_3**

tolerance tests, as well as metabolic cage (PhenoMaster^{NG}, Bad Homburg, Germany), assays as scheduled in Fig. 2a. After 3 weeks, all mice were euthanized after 12 h of fasting, followed by the collection of blood and tissue samples.

Frozen or paraffin-embedded sections (5-μm) of the liver were prepared as previously described and were stained with Oil red O to determine lipid accumulation, or Hematoxylin-Eosin (H&E) to determine hepatic structure [26], respectively. Hepatic free fatty acids (FFA) and triglycerides (TG) levels were determined using an FFA assay kit (Cat#: BC0595, Solarbio, Beijing, China) and LabAssay™ triglyceride kit (Cat# 290–63701, WAKO, Japan), respectively. The activities of alkaline phosphatase (ALP), alanine aminotransferase (ALT), and aspartate aminotransferase (AST), as well as the levels of TG, FFA, cholesterol, high-density lipoprotein cholesterol, and low-density lipoprotein cholesterol in the serum, were analyzed using an automated biochemical analyzer (3100, Hitachi High-Technologies Corporation, Tokyo, Japan).

Immunohistochemistry staining and immunofluorescence staining
After preparation of hepatic paraffin and frozen sections, immunohistochemistry staining and immunofluorescence staining were performed according to the previous protocol [27], respectively. Meanwhile, negative-control (NC) was applied to each experiment, in which the corresponding normal IgG was used instead of primary antibodies, and no other steps were changed. After the images were acquired by ZEISS Scope A1 fluorescence microscope (Oberkochen, Germany), statistical analysis was performed using Image J software. To determine mean density or mean fluorescence intensity (MFI) of the positive staining area, the integrated optical density of a region and the area of the region were detected for each section ($n = 5$), followed by calculating the ratio of the two values to reflect the expression of the target protein per unit area. The final result was expressed as fold changes compared to the control group [28].

Dihydroethidium (DHE) staining
DHE staining was performed using frozen sections to determine hepatic superoxide levels. Briefly, after washing with PBS, frozen sections were incubated with DHE (10 μM) for 30 min at 37 °C, followed by washing again and then photographed with ZEISS Scope A1 fluorescence microscope (Oberkochen, Germany). The MFI of the positive staining area was calculated as described in the *Immunohistochemistry staining and immunofluorescence staining* section.

Western blot
For cell or tissue samples, proteins were extracted with the protein lysis buffer containing protease inhibitor (PMSF and cocktail). Protein expression of Nogo-B, NgBR, ACC, FASN, ChREBP, SOD1, SOD2, NRF2, NLRP3, pNF-κB, NF-κB, IL-1β, pIRS1, IRS1, pAKT, AKT, αSMA, TGFβ, P62, Beclin1, LC3B, pmTOR, mTOR, pAMPKα, AMPKα were detected by Western blot as described [29]. The blots were normalized using β-actin or HSP90 as the loading control. For quantitative analysis of the band density, all results of Western blot were scanned by Photoshop software and normalization by the density of loading control molecule in the corresponding samples.

Preparation of Nogo-B expression vector and transfection
Human Nogo-B cDNA (NM_138459.5) was cloned into the pEGFP-C2 vector (Clontech, Mountain View, CA, USA) by total gene synthesis in Tsingke Biotechnology (Beijing, China) and named as EGFP-Nogo-B. When HepG2 cells reached 70%–80% cell density in 6-well plates, the medium was replaced with fresh complete medium without antibiotics, followed by transfection of EGFP-Nogo-B or corresponding control (2 μg/well) using liposome transfection reagent (6 μg/well). After 12 h of transfection, cells were switched to serum-free medium containing FA-fructose mixture (as described in the *Cell culture* section) with/without 6-MF and incubated for 24 h. Cells were subsequently collected to extract total protein.

Oil red O and ROS staining of cells
In 24-well plates, HepG2 cells with/without overexpression of Nogo-B (~10^5 cells/well) were seeded on cover slips, followed by dividing each type of cell into three groups (5 wells/group). After attachment, as described in the *Cell culture* section, cells were induced by FA-fructose mixture to construct the cellular model of liver injury and treated with/without 6-MF for 24 h in both types of cells, respectively. Then cells were stained with Oil Red O solution at the end of treatment [26] as described.

As for ROS staining, cells were washed with PBS after treatment, and endogenous ROS was detected using the DCFH-DA (MB4682, Meilunbio, Dalian, China), a cell-permeable probe for ROS. The cells were incubated with a PBS solution containing 5 μM DCFH-DA at 37 °C in dark for 30 min, and then photographed by the fluorescence microscope.

Determination of oxygen consumption rate (OCR) in HepG2 cells
Determination of the OCR in HepG2 cells was conducted using an XFp extracellular flow analyzer (Agilent, USA) with the corresponding kits (103010–100, Agilent, USA). Briefly, HepG2 cells were seeded onto dedicated 8-well plates at a density of ~10^4 cells/well (two wells used as controls without cell inoculation). Outside of the control, cells were all treated with an FA-fructose mixture with or without 6-MF simultaneously and incubated at 37 °C for 24 h. Thereafter, cells were washed using an assay medium containing 1 mM pyruvate, 2 mM glutamine, and 10 mM glucose three times, followed by incubation in assay medium for 1 h at 37 °C in a non-CO_2 incubator. The OCR was determined by the sequential addition of 1.5 μM oligomycin (ATP synthase inhibitor), 1 μM carbonyl cyanide p-trifluoromethoxy-phenylhydrazone (FCCP, oxidative phosphorylation uncoupler), and 0.5 μM rotenone/antimycin A (Rot/AA) to the cells. Throughout each conditional cycle, real-time OCR values were obtained and averaged in triplicate. The values of OCR were normalized to the number of cells.

TUNEL staining
The TUNEL BrightRed Apoptosis Detection Kit (Cat# A113–03, Vazyme, Nanjing, China) was used to detect cell death in paraffin sections of liver as described [30]. NC and positive control were set up to exclude interference from non-test factors, separately. Images were observed by ZEISS Scope A1 fluorescence microscope (Oberkochen, Germany) and liver apoptosis was determined by comparing the number of positive cells.

Analysis of autophagic flux
HepG2 cells were transfected with AdPlus-mCherry-GFP-LC3B adenoviral vector (C3012, Beyotime, Shanghai, China), and the autophagic flux was reflected by detecting the red and green fluorescence in the cells. Mechanistically, the green fluorescence of GFP is quenched in the acidic environment during the fusion of autophagosome with lysosomes, while the red fluorescence of mCherry is retained owing to its superior stability. Thus, after autophagy occurs, mCherry-GFP-LC3B under fluorescence microscopy appears as red spots due to partial quenching of GFP fluorescence. And when autophagy is suppressed, mCherry-GFP-LC3B under fluorescence microscopy appears as yellow spots. To determine the effect of FA-fructose mixture and 6-MF treatment on the autophagic flux of HepG2, HepG2 cells were seeded in confocal dishes (10^5 cells/well), incubated in 1 mL of medium containing adenovirus (20 MOI) for 6 h, followed by transfection with fresh complete medium for 48 h. Afterwards, the cells were induced injury as described in *Cell culture* and detected by Leica laser confocal microscopy (Wetzlar, Hesse-Darmstadt, German). The MFI of yellow spots was calculated as described in the *Immunohistochemistry staining and immunofluorescence staining* section.

Detection of cellular ability to degrade lipids by autophagy
The ability of cells to degrade lipids is reflected by autophagosomes and lipid colocalization. HepG2 cells were seeded into confocal dishes (~10^5 cells/well) and treated with 6-MF or FA-fructose mixture individually or together as described in the *Cell culture* section. After treatment, HepG2 cells were fixed using 4% paraformaldehyde for 30 min and washed three times with PBS. Thereafter, HepG2 cells were permeabilized in 0.1% Triton-X-100 for 10 min, washed three times, and blocked with 3% bull serum albumin at room temperature for 1 h. HepG2 cells were then incubated with LC3B antibody overnight at 4 °C. Cells were washed the next day with PBS and incubated alongside the FITC-conjugated secondary antibody at room temperature for 2 h, followed by PBS washing and staining with Nile Red (2 μg/mL) at room temperature for 30 min. After DAPI staining, images were acquired using a Leica laser confocal microscope (Wetzlar, Hesse-Darmstadt, German). The MFI of the corresponding fluorescence was calculated as described in the *Immunohistochemistry staining and immunofluorescence staining* section.

Statistical analysis
All data analysis was performed by a technician who is blind to the experimental design and was expressed as the mean ± SEM of each group or normalized to the mean of the experimental control group. All data were analyzed by normality and equal variance to determine whether Prism software performed parametric or nonparametric analysis. Two-tailed Student's *t* tests were conducted among two groups, and one-way ANOVAs with post-hoc tests were conducted among more than two groups. The two-way ANOVA with post-hoc test was used to analyze the data that included two variables. In the analysis, a significant difference is considered when $P < 0.05$.

RESULTS

Screening and validation of flavonoids inhibiting the expression of Nogo-B
Based on the critical pathophysiological role of Nogo-B and its potential to become a therapeutic target as well as the general biological activity and therapeutic properties of flavonoids, we selected 14 flavones/isoflavones with relatively simple structures (Table 1) to screen for compounds capable of inhibiting Nogo-B expression within hepatocytes. As shown in Figure S1a, all

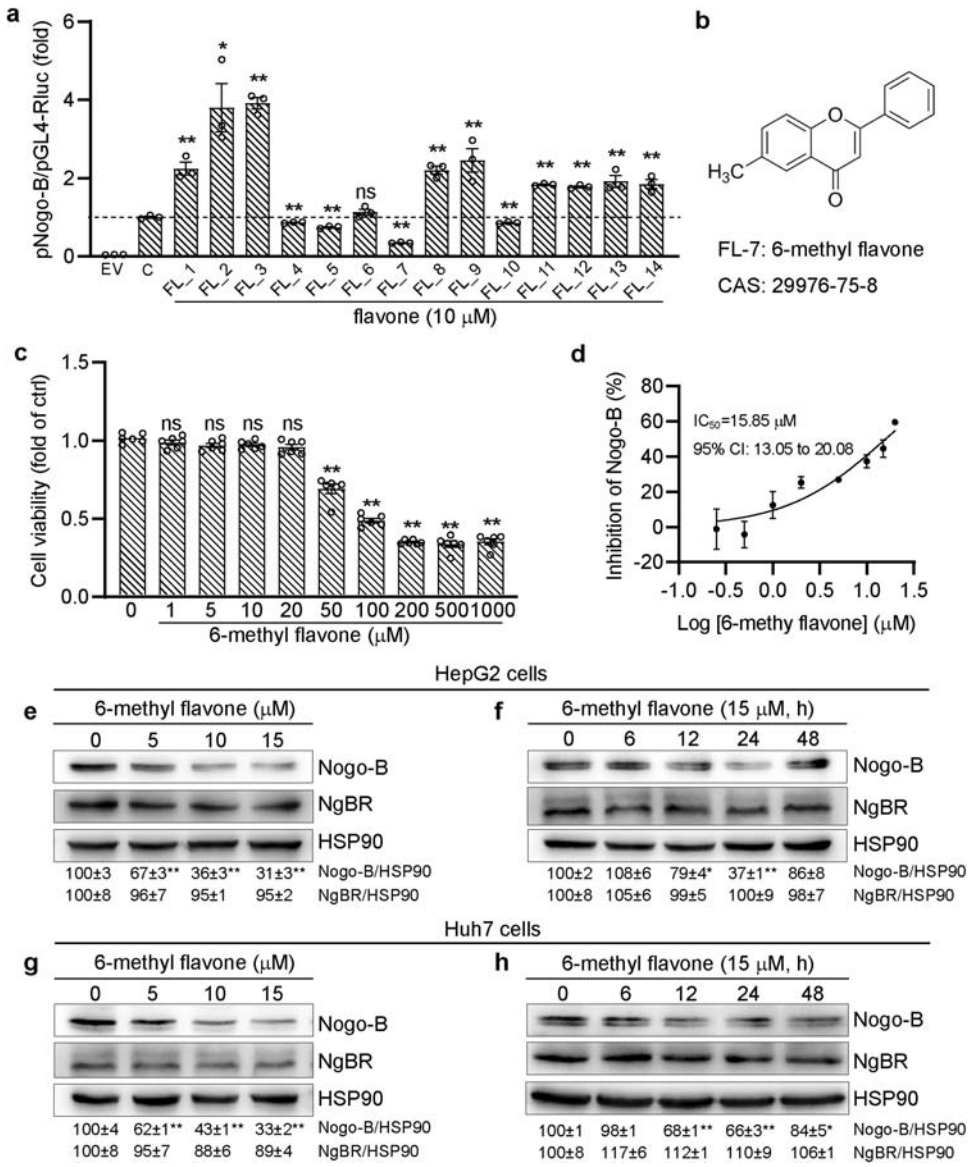

Fig. 1 6-Methyl flavone (6-MF) inhibits the expression of Nogo-B. a HepG2 cells were treated with 10 μM of flavonoids for 24 h followed by detecting the relative luciferase activity of Nogo-B promoter ($n = 3$). **b** Chemical structure of 6-MF. (**c**) HepG2 cells were treated with 6-MF for 24 h followed by determining cell viability by MTT assay ($n = 6$). (**d**) Dose–response curve reflects the inhibitory effect of 6-MF in HepG2 cells after treatment for 24 h ($n = 6$). The IC_{50} was calculated by fitting percentage inhibition values and log of compound concentrations to nonlinear regression (dose response–variable slope) with Graphpad 9.0. **e–h** The expressions of Nogo-B and NgBR were analyzed by Western blot in HepG2 cells (**e**, **f**) or Huh7 cells (**g**, **h**) treated with 6-MF at the gradient concentrations for 24 h (**e**, **g**) or with 15 μM 6-MF for the gradient time (**f**, **h**) ($n = 3$). All data are presented as the mean ± SEM, $^{*}P < 0.05$, $^{**}P < 0.01$.

flavonoids did not have obvious cytotoxicity at a concentration of 10 μM (the majority of flavonoid concentrations commonly used was 10 μM in vitro [21, 22]) in HepG2 cells. We evaluated the ability of 14 flavonoids at 10 μM to inhibit the Nogo-B promoter activity through a dual luciferase reporter system, and FL_7 (6-methyl flavone, CAS: 29976-75-8) exhibited the strongest inhibitory effect (Fig. 1a, b). MTT assays indicated that 6-methyl flavone (6-MF) was significantly cytotoxic above a concentration of 50 μM (Fig. 1c). Therefore, we determined the effects of 6-MF using a concentration gradient (0.25, 0.5, 1, 2, 5, 10, 15, 20 μM) on the Nogo-B promoter activity and found the 50% inhibitory concentration (IC_{50}) of 6-MF to be 15.85 μM (Fig. 1d). To further clarify the inhibitory effect of the compounds, we examined the effect of 6-MF on Nogo-B protein levels in HepG2 and Huh7 cells, respectively. The results demonstrated that in both HepG2 and Huh7 cells, 6-MF was able to inhibit Nogo-B expression in a concentration-dependent and time-dependent manner without impacting NgBR levels (Fig. 1e, f), suggesting that 6-MF inhibits Nogo-B independently of NgBR. Overall, 6-MF may be a potentially effective compound for inhibiting Nogo-B expression in vitro.

6-MF improves HFrD-induced metabolic disorders and liver injury in C57BL/6J mice

Previous studies have demonstrated that Nogo-B is a core molecule affecting hepatic glycolipid metabolism which is upstream of ChREBP, suggesting that it may be a novel target for the treatment of metabolic syndrome [15]. Because 6-MF can inhibit Nogo-B in vitro, we speculated that it could inhibit hepatic Nogo-B in vivo to improve HFrD-induced metabolic disorders and liver injury. Therefore, as shown in Fig. 2a, we separated C57BL/6J into four groups and conducted the experiments as planned. Mice in the NC-C or NC-F groups were fed normal food and treated with

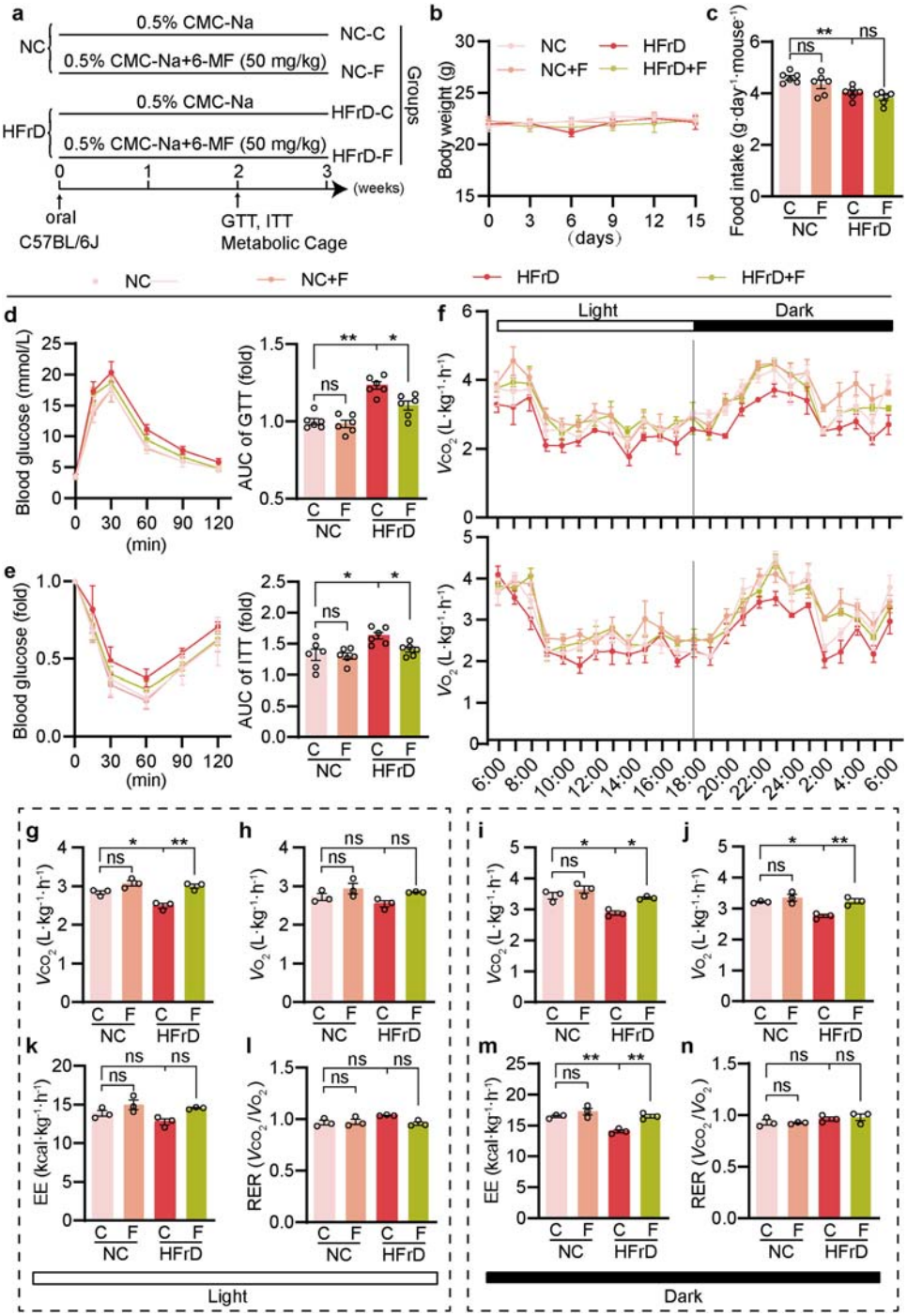

Fig. 2 6-MF ameliorates HFrD-induced metabolic disorders. a Mice were assigned to the four groups and received the indicated treatment. After 3-week treatment, mice were conducted the following assays. **b** The body weight of mice was measured every three days ($n = 6$). **c** Daily food intake of mice ($n = 6$). The glucose tolerance test (GTT) (**d**) or insulin tolerance test (ITT) (**e**) was performed before the end of the experiment. Blood glucose levels were determined at the indicated time points after glucose or insulin administration with quantitation of area under curve (AUC) ($n = 6$). (**f**) The curves of CO_2 production and O_2 consumption during a 24-h light–dark cycle ($n = 3$). The CO_2 production and the O_2 consumption in light (**g**, **h**) and dark (**i**, **j**) by mice ($n = 3$). The energy expenditure (EE) and respiratory exchange rate (RER) in light (**k**, **l**) and dark (**m**, **n**) by mice ($n = 3$). All data are presented as the mean ± SEM, $^*P < 0.05$, $^{**}P < 0.01$, ns: not significant.

CMC-Na (0.5%, i.g, NC-C) or 6-MF (50 mg/kg, i.g, HC-F). Mice in the HFrD-C or HFrD-F groups were fed HFrD and treated with CMC-Na (0.5%, i.g, HFrD-C) or 6-MF (50 mg/kg, i.g, HFrD-F).

Throughout the treatment, mice fed an HFrD consumed less food, while 6-MF did not impact body weights (Fig. 2b) and food intake (Fig. 2c). To confirm whether insulin sensitivity was altered, we performed GTT, and ITT, and detected the insulin and glucose levels. Compared to the NC-C group, the area under the curve (AUC) for both GTT and ITT was significantly higher in the HFrD-C group, suggesting that HFrD resulted in insulin resistance (Fig. 2d, e, NC-C *vs.* HFrD-C). In contrast, 6-MF recovered the insulin sensitivity (Fig. 2d, e, HFrD-C *vs.* HFrD-F). Additionally, 6-MF restored the elevated insulin and glucose levels caused by HFrD (Fig. S1b, c). At the molecular level, 6-MF improved the phosphorylation of IRS1

and Akt compared to the HFrD-C group (Fig. S2a). Overall, while fructose may be used as an energy source, excess fructose can cause liver damage, and 6-MF may improve hepatic insulin resistance and hyperinsulinemia caused by an HFrD.

In addition to impairing glucose tolerance, HFrD also impacts energy metabolism. To assess the effect of 6-MF on whole-body energy metabolism, the respiration rate (RER) and energy expenditure (EE) of the four groups were obtained using metabolic cages. An HFrD slightly reduced carbon dioxide production (V_{CO_2}), and significantly reduced oxygen consumption (V_{O_2}) in the dark, which may be due to the predominantly nocturnal activity of mice. 6-MF increased both V_{CO_2} and V_{O_2} (Fig. 2f–j, HFrD-C *vs*. HFrD-F) and the energy expenditure (EE) (Fig. 2k, m, HFrD-C *vs*. HFrD-F), suggesting that 6-MF enhanced basal metabolism in mice. However, no change in the respiratory exchange rate (RER) was observed (Fig. 2l, n), indicating that the material sources of energy are the same. These results related to V_{CO_2}, V_{O_2}, and EE indicated that 6-MF can improve HFrD-induced abnormalities in energy metabolism.

Excess fructose can be a raw material for fatty acid synthesis, potentially increasing the risk of NAFLD [31]. Correspondingly, fructose-induced fatty acid production triggers an inflammatory response and oxidative stress in hepatocytes, which can contribute to liver damage [32, 33]. As observed in Fig. 3a, the liver color of HFrD-fed mice was whiter. 6-MF restored this color change (Fig. 3a), and decreased the ratio of liver weight to body weight compared to HFrD-C group (Fig. 3b). The results of H&E and Oil red O staining demonstrated severe vacuolar droplets, infiltration of inflammatory cells, and lipid accumulation in the liver of the HFrD-C group mice (Fig. 3c, NC-C *vs*. HFrD-C). All of these metrics were substantially reduced in mice in the HFrD-F group (Fig. 3c, HFrD-C *vs*. HFrD-F). In addition, we evaluated the levels of TG and FFA in the liver and serum. 6-MF significantly ameliorated the increase of lipid content caused by HFrD (Fig. 3d–g). Liver injury was assessed by measurement of ALP, ALT, and AST levels in the serum. Compared to the HFrD-C group, 6-MF restored the elevated ALP, ALT, and AST levels (Fig. 3h–j). In contrast, the levels of various cholesterol, total protein, and albumin (ALB) were not improved by 6-MF (Fig. S1d–h). Figures 2, 3 demonstrated that 6-MF protects mice from HFrD-induced insulin resistance and improves both hepatic lipid accumulation and hypertriglyceridemia.

6-MF inhibits lipid synthesis, oxidative stress, and inflammatory responses in the liver along with decreased Nogo-B expression

Studies have demonstrated that Nogo-B is not expressed or expressed at low levels in normal hepatic parenchymal cells, but it

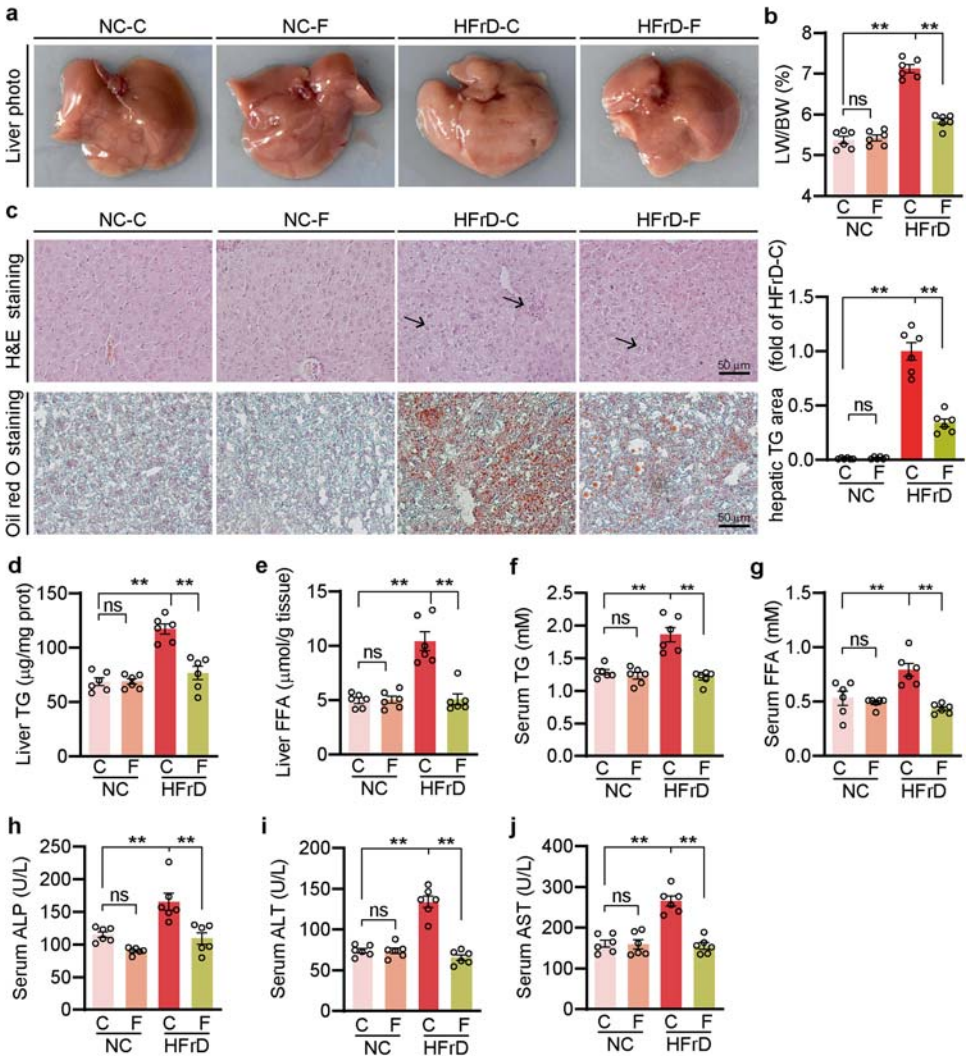

Fig. 3 6-MF ameliorates HFrD-induced liver injury and hyperlipidemia. a Photos of mice liver. **b** The ratio of liver weight to bodyweight ($n = 6$). **c** H&E staining of liver paraffin sections and with an arrow indicates inflammatory cells in the liver, Oil red O staining of liver frozen sections and statistical analysis of TG area. Quantitative analysis of liver TG (**d**) and FFA (**e**) with total liver lipid extract ($n = 6$). The levels of TG (**f**), FFA (**g**), ALP (**h**), ALT (**i**), AST (**j**) in serum ($n = 6$). All data are presented as the mean ± SEM, $^{**}P < 0.01$, ns: not significant.

is significantly increased when cells are stimulated or damaged. Nogo-B can be secreted into the blood and may impact multiple tissues via the circulatory system [10]. To confirm that 6-MF has a Nogo-B-reducing effect in vivo, we determined the Nogo-B level in both the serum and liver. This was possibly caused by low Nogo-B expression, and 6-MF did not alter circulating and hepatic Nogo-B levels under normal dietary conditions. However, 6-MF significantly reduced Nogo-B levels in the serum and liver of the HFrD-fed mice (Fig. 4a–c). We determined the expression of Nogo-B across other tissues and Nogo-B expression was unchanged in the brain, kidney, muscle, gut, pancreas, and adipose tissue (Fig. S2b–g).

Fructose is critical for the activation of ChREBP to upregulate the expression of genes related to lipid synthesis, and excess synthesis and accumulation of fatty acids in the liver may cause lipotoxicity [34]. Compared to the NC-C group, HFrD increased the expression of fatty acid synthase (FASN), Acetyl-CoA Carboxylase (ACC), and ChREBP, but 6-MF rescued this change (Fig. 4d, e). Similarly, the immunofluorescence results indicated that 6-MF improved the HFrD-induced high expression and nuclear translocation of ChREBP (Fig. 4f). Furthermore, the excess FFA and high metabolic activity of fructose induce large amounts of reactive oxygen species (ROS), causing intense oxidative stress and inflammatory responses [35]. We determined the level of hepatic superoxide through DHE staining and found that 6-MF could reduce the high level of superoxide which was induced by HFrD (Fig. 4g). 6-MF significantly up-regulated the levels of superoxidase dismutase 1 (SOD1) and SOD2 in the HFrD-fed mouse liver, indicating that 6-MF possesses anti-oxidative stress effects (Fig. 4h). Compared to the HFrD-C group, 6-MF reduced the serum levels of inflammatory factors (Fig. 4i) and decreased the inflammatory response in the liver through inhibition of the NF-κB signaling pathway (Fig. 4j, k). Associated with the inhibition of ROS and proinflammatory factors, 6-MF inhibited apoptosis of liver cells (Figure S3a). Ultimately, 6-MF significantly reduced the hepatic Nogo-B upregulation induced by HFrD and inhibited lipid synthesis, oxidative stress, and inflammatory responses in the liver.

6-MF inhibits lipid synthesis, oxidative stress, and inflammatory responses induced by an FA-fructose mixture in HepG2 cells

To verify the effects and mechanism of 6-MF in improving fructose-induced liver injury, we created an in vitro model of liver injury using a mixture of fructose and fatty acids (FA, palmitic acid/oleic acid = 2/1) in HepG2 cells treated for 24 h to mimic the conditions of HFrD-induced liver injury in mice. The results indicated that Nogo-B expression in HepG2 cells was enhanced by the FA-fructose mixture in a concentration-dependent manner (Fig. 5a, top panel). Additionally, the expression of lipogenesis genes (FASN, ACC, ChREBP) was increased and the expression of antioxidant-related genes (SOD1, SOD2) was reduced (Fig. 5a, middle and lower panel). Cellular ROS (Fig. 5b, c) and medium TNF-α (Fig. 5d) levels were also enhanced through stimulation with an FA-fructose mixture. However, 6-MF reduced the expression of Nogo-B and lipogenesis genes while restoring the levels of SOD1 and SOD2 (Fig. 5e). Compared to the modeling group, 6-MF also reduced ROS (Fig. 5f, g) and cell-secreted TNF-α (Fig. 5h) levels.

To further investigate if the therapeutic effect of 6-MF operates through the inhibition of Nogo-B, we overexpressed Nogo-B in HepG2 cells. 6-MF was able to inhibit the expression of endogenous Nogo-B (Fig. 5i, top panel), but had limited effect on the lipogenesis and antioxidant gene expression (Fig. 5i, middle and lower panel). 6-MF was also unable to inhibit intracellular ROS (Fig. 5j, k) and medium TNF-α (Fig. 5l) levels in the presence of Nogo-B overexpression. Additionally, the FA-fructose mixture or Nogo-B overexpression stimulated cells to deposit more lipid droplets, while 6-MF reduced lipid accumulation in control cells, but not in Nogo-B overexpressing cells (Fig. S3b). Therefore, these data indicate that 6-MF may improve high fructose-induced liver injury through Nogo-B inhibition.

6-MF restores HFrD-inhibited cellular autophagy to improve liver injury

Previous studies have demonstrated that Nogo-B knockout inhibited the activation of ChREBP through high fructose and subsequent lipid synthesis [15]. We speculate that 6-MF also inhibits lipid synthesis *via* the Nogo-B-ChREBP pathway, ameliorating HFrD-induced liver injury. To verify this, we overexpressed ChREBP in HepG2 cells and treated them with an FA-fructose mixture and 6-MF. Although ChREBP overexpression abolished the effect of 6-MF on lipid synthesis, it still activated antioxidant-related genes (Fig. 6a). Correspondingly, intracellular ROS (Fig. 6b, c) and cell-secreted TNF-α (Fig. 6d) levels were reduced by 6-MF under ChREBP overexpression. These imply that the therapeutic effect of 6-MF may not be achieved exclusively through inhibiting lipid synthesis and reducing cellular lipid levels.

Cellular respiration, reflecting the function of mitochondrial oxidative phosphorylation, is the process by which organic compounds are oxidized and energy is released within the cell. Fatty acids, glucose, and amino acids are the main substrates for oxidative phosphorylation. Through the detection of the oxygen consumption rate (OCR) of HepG2 cells (Fig. 6e), we found that 6-MF increased basal respiration, maximal respiration, proton leakage, and ATP production (Fig. 6f) compared to the FA-fructose mixture alone. We hypothesize that 6-MF promoted fatty acid β-oxidation. In addition, 6-MF increased the level of carnitine palmitoyl transferase 1α (CPT1α), the key rate-limiting enzyme for fatty acid oxidation, in both mouse livers and HepG2 cells (Fig. 6g, h). These data indicate that 6-MF activated lipid β-oxidation, also contributing to improved lipid accumulation in the injured liver.

Catabolism of lipid droplets *via* autophagy followed by the promotion of β-oxidation of FFA is considered a central regulator of hepatic lipid metabolism [36]. Mice on a high-fat or high-carbohydrate diet frequently exhibit impaired hepatic autophagy and dysregulation of autophagy is strongly associated with NAFLD [37, 38]. To connect the relationship between 6-MF and autophagy, we detected the expression of autophagy-related genes (Beclin1, P62, LC3B) both in vivo and in vitro. We observed that 6-MF reduced the expression of P62, a specific substrate of autophagy [39], increased by HFrD (Fig. 6g, i). Beclin1 is a crucial regulator of autophagy, and the ratio of LC3BII/LC3BI may reflect the level of autophagy [39]. HFrD decreased Beclin1 expression and the LC3BI/LC3BII ratio, while 6-MF reversed the change (Fig. 6g, i). In HepG2 cells, we confirmed that the FA-fructose mixture inhibited autophagy (Fig. S4a), and 6-MF rescued the damaged autophagy (Fig. 6h). Therefore, these results indicate that in addition to inhibiting lipid synthesis, 6-MF ameliorates high fructose-induced lipid accumulation through the restoration of impaired autophagy.

6-MF activates HFrD-damaged autophagy via the AMPKα-mTOR pathway

To further confirm the impact of 6-MF on autophagic flux in hepatocytes, we transfected HepG2 cells with mCherry-GFP-LC3B adenovirus. This adenoviral vector results in both green and red colors (yellow after merging) in the autophagosome, while in the autolysosome it only emits red due to the acidic hydrolysis of GFP. After 24 h of treatment with the FA-fructose mixture, the number of cells exhibiting red fluorescence in the merged graph was reduced, while the number of cells exhibiting yellow fluorescence was enhanced compared to the control group, suggesting that autophagic flux was inhibited (Fig. 7a, b, FF vs. Ctrl). 6-MF restored the autophagy of the cells to normal levels (Fig. 7a, FF + 6-MF vs. FF). Moreover, we observed that the lipid content of the cells was significantly enhanced by the FA-fructose mixture, while the number of autophagosomes was decreased overall (Fig. 7c, d, FF vs. Ctrl).

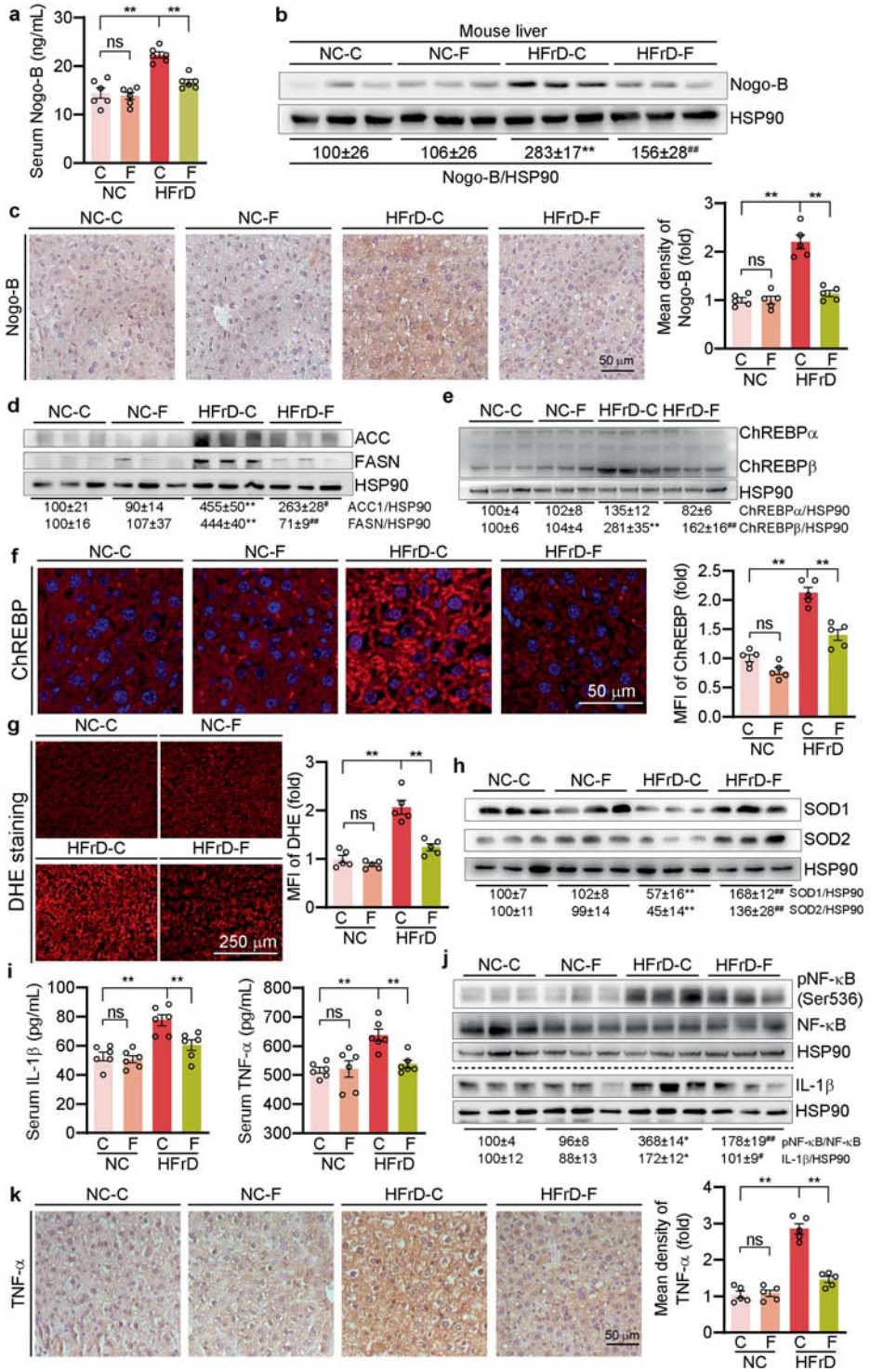

Fig. 4 6-MF decreased Nogo-B expression along with inhibiting lipid synthesis, oxidative stress, and inflammatory responses in the liver. **a** Serum Nogo-B levels were determined by Elisa kit ($n = 6$). Hepatic Nogo-B expression was determined by Western blot ($n = 3$) (**b**) and immunohistochemistry staining (**c**) ($n = 5$). Protein expression of ACC, FASN (**d**) and ChREBPα/β (**e**) in liver was determined by Western blot ($n = 3$). **f** Immunofluorescent staining of liver sections for determination of ChREBP ($n = 5$). **g** Superoxide in liver was determined by DHE staining. ($n = 5$). **h** Protein expression levels of SOD1 and SOD2 in liver were determined by Western blot ($n = 3$). **i** Serum levels of IL-1β and TNFα in groups were determined by Elisa kits ($n = 6$). **j** Protein expression of pNF-κB, NF-κB, and IL-1β in liver was determined by Western blot ($n = 3$). **k** Immunohistochemistry staining of liver sections for determination of TNF-α ($n = 5$). All data are presented as the mean ± SEM, $^{*}P < 0.05$, $^{**}P < 0.01$, ns: not significant. For the quantitation of the band density, $^{*}P < 0.05$, $^{**}P < 0.01$ vs. NC-C, $^{\#}P < 0.05$, $^{\#\#}P < 0.01$ vs. HFrD-C.

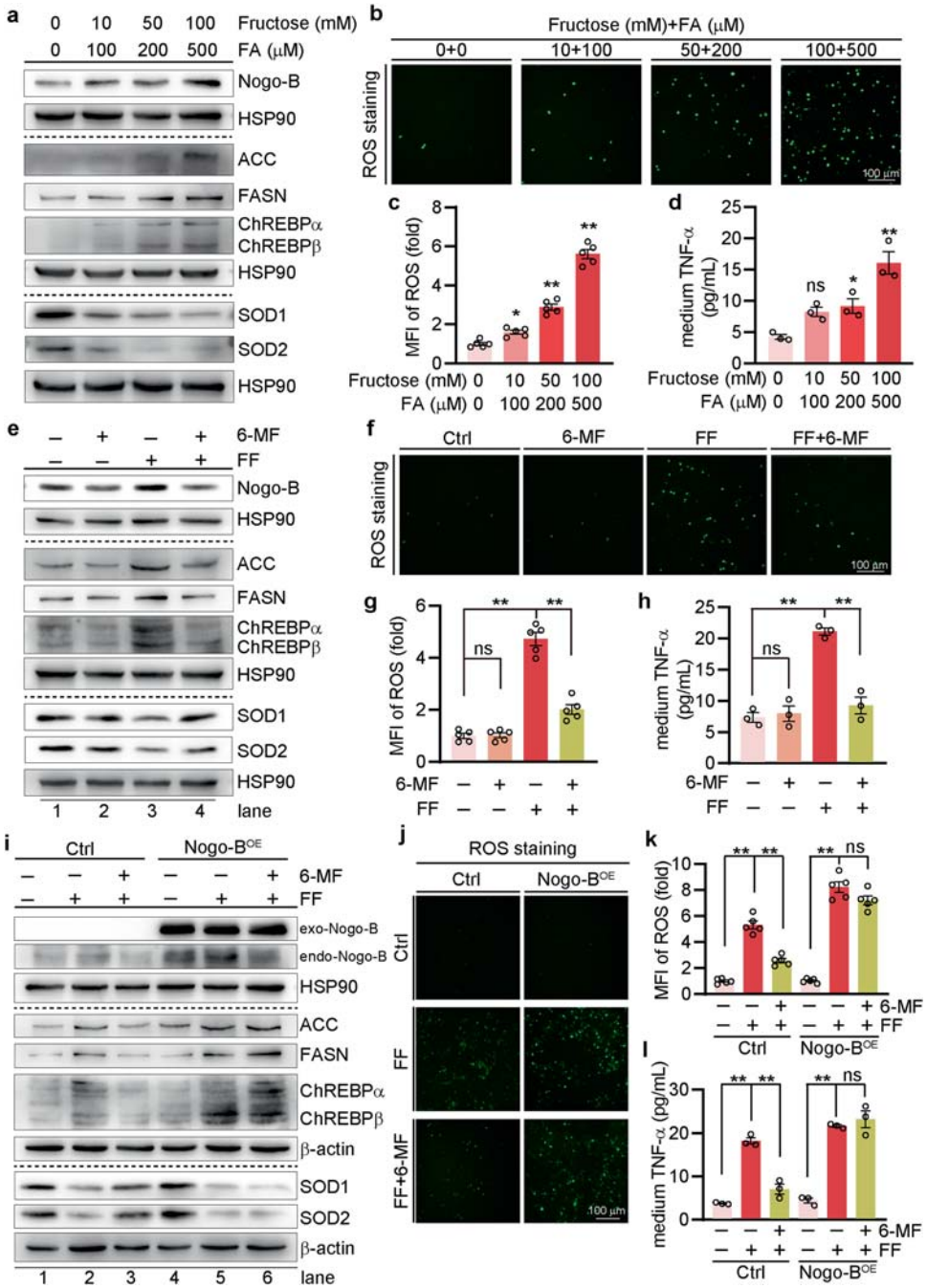

Fig. 5 6-MF inhibits lipid synthesis, oxidative stress and inflammatory responses in HepG2 cells. a–d HepG2 cells were incubated with a gradient concentration of the FA-fructose mixture for 24 h. **e–h** HepG2 cells treated by 15 μM 6-MF with/without FA-fructose mixture (FA: 100 mM, fructose: 500 μM) stimulation for 24 h. **i–l** In the condition of normal (lane 1–3) and Nogo-B overexpression (lane 4–6), HepG2 cells were stimulated by FA-fructose mixture (FA: 100 mM, fructose: 500 μM) and treated with 15 μM 6-MF for 24 h. After the different treatments described above, cells and medium were used to complete the following experiments: (**a**, **e**, **i**) Protein expression levels of Nogo-B, ACC, FASN, ChREBPα/β, SOD1 and SOD2 were determined by Western blot ($n = 3$). (**b**, **c**; **f**, **g**; **j**, **k**) Cellular ROS staining (**b**) and the mean fluorescence intensity (MFI) of ROS (**c**) ($n = 5$). (**d**, **h**, **l**) Medium TNF-α level was determined by Elisa kit ($n = 5$). All data are presented as the mean ± SEM, $^*P < 0.05$, $^{**}P < 0.01$, ns: not significant. The quantitation results of the band density in **a**, **e** and **i** were displayed in supplemental information (Table S1).

6-MF increased the amount of co-localization of autophagosomes and lipids [Fig. 7c (Merge), FF + 6-MF vs. FF], suggesting increased lipid autophagy and reduced cellular lipid content.

Next, we examined the classical signaling pathways involved in the regulation of autophagy levels. The AMP-activated protein kinase α (AMPKα) signaling pathway, acting as the center of regulation of energy metabolism, can activate cellular autophagy by inhibiting the phosphorylation of the mammalian target of rapamycin (pmTOR) [40]. It was found that hepatic phosphorylation of AMPKα (pAMPKα) was significantly inhibited in the HFrD-C group alongside concomitant activation of mTOR (Fig. 7e, NC vs. HFrD-C), whereas 6-MF rescued the inhibition of AMPKα and suppressed the level of pmTOR (Fig. 7e, HFrD-C vs. HFrD-F). In HepG2 cells, the FA-fructose mixture inhibited AMPKα phosphorylation and activated mTOR (Fig. S4b), while 6-MF rescued this change (Fig. 7f).

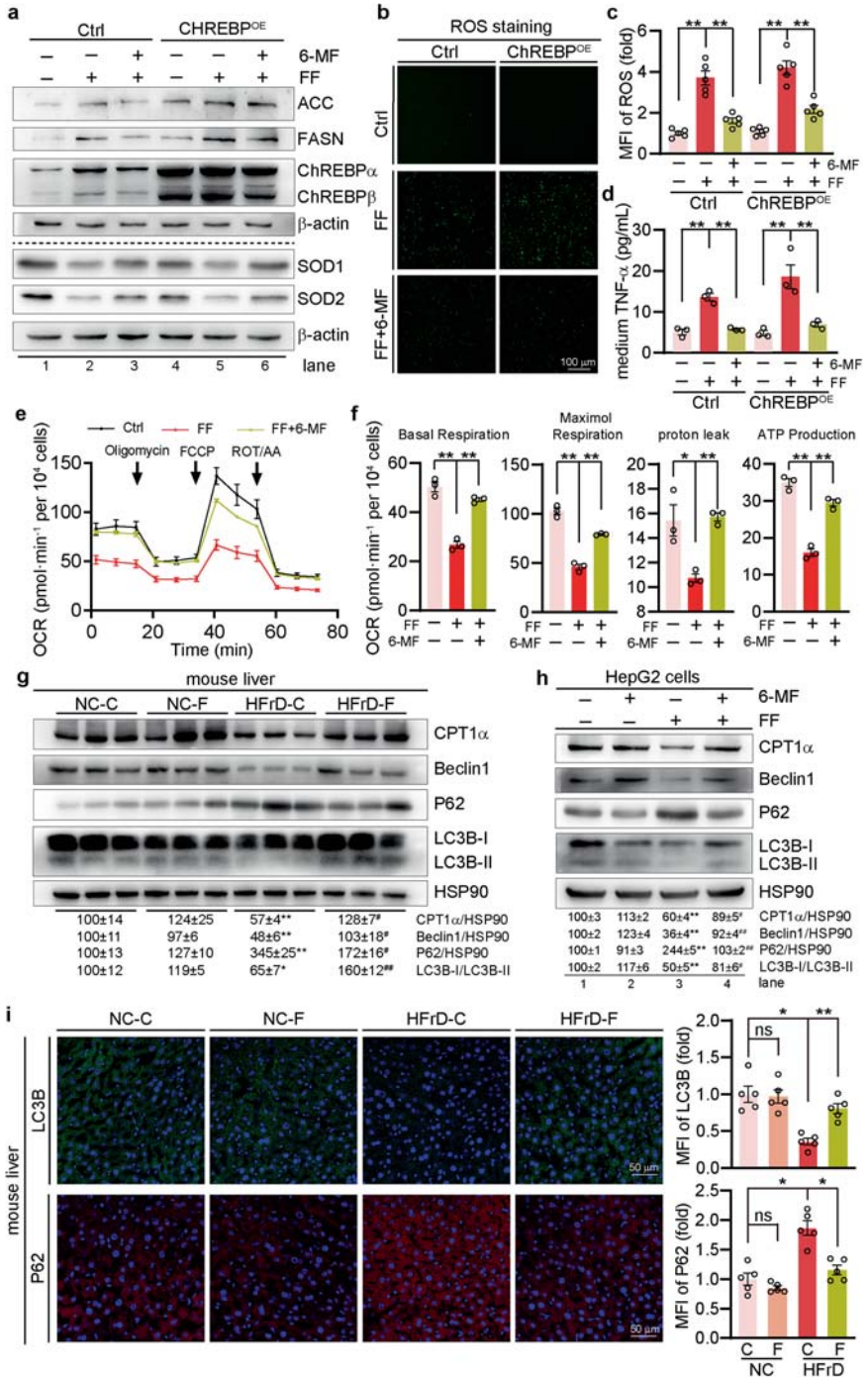

Fig. 6 6-MF restores HFrD-inhibited β-oxidation and cellular autophagy. a–d In the condition of normal (lane 1–3) and ChREBP overexpression (lane 4–6), HepG2 cells were stimulated by FA-fructose mixture (FA: 100 mM, fructose: 500 μM) and treated with 15 μM 6-MF for 24 h. After the treatment, cells and medium were used to complete the following experiments: **a** Protein expression levels of ACC, FASN, ChREBPα/β, SOD1 and SOD2 were determined by Western blot ($n = 3$). The quantitation results of the band density in **a** were displayed in supplemental information (Table S1). Cellular ROS staining (**b**) and the mean fluorescence intensity (MFI) of ROS (**c**) ($n = 5$). **d** Medium TNF-α level was determined by Elisa kit ($n = 5$). **e**, **f** The OCR was monitored over the sequential injection of oligomycin (1 μM), FCCP (1.5 μM) and Rot/AA (0.5 μM) (n = 3). **g**, **h** Protein expression of CPT1α, Beclin1, P62 and LC3B in liver (**g**) and HepG2 cells (**h**) were determined by Western blot ($n = 3$). **i** Immunofluorescent staining of liver sections for determination of LC3B and P62 ($n = 5$). All data are presented as the mean ± SEM, $^{*}P < 0.05$, $^{**}P < 0.01$, ns: not significant. For the quantitation of the band density, $^{*}P < 0.05$, $^{**}P < 0.01$ vs. NC-C/lane 1, $^{\#}P < 0.05$, $^{\#\#}P < 0.01$ vs. HFrD-C/lane 3.

We treated cells with AMPK inhibitor Compound C (10 μM) to further determine whether 6-MF enhances autophagic flux *via* the AMPKα-mTOR pathway. The results demonstrated that Compound C did not alter Nogo-B expression (Fig. S4c), and 6-MF failed to activate AMPKα and inhibit pmTOR expression after inhibitor treatment (Fig. 7g). Cellular β-oxidation was hindered and autophagy levels were lowered after inhibitor treatment alone compared to normal treatment (Fig. 7h, lane 1 vs. lane 4). The inhibition of autophagy and β-oxidation was exacerbated by the FA-fructose mixture, and 6-MF was unable to rescue the impairment of autophagy under Compound

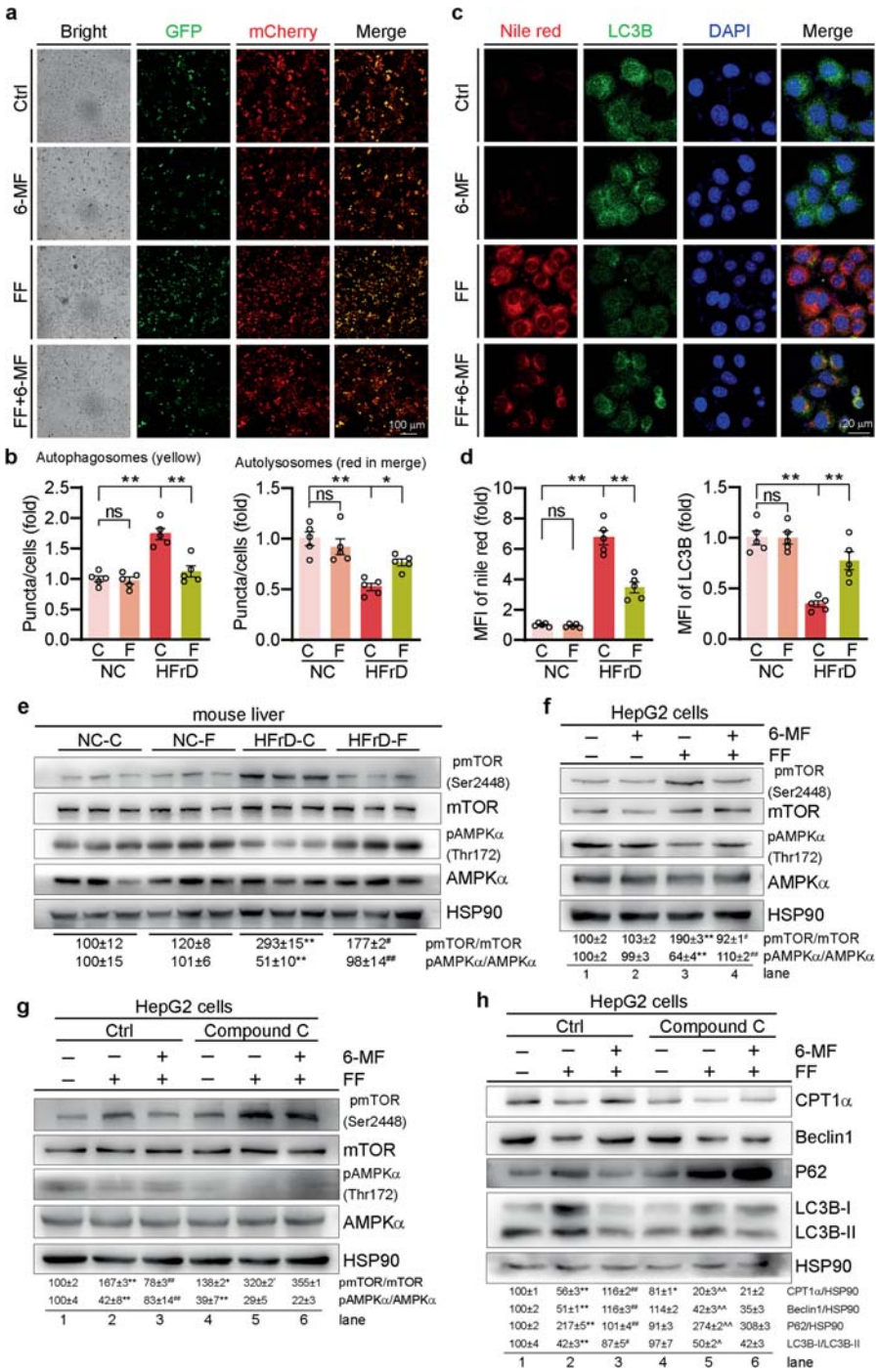

Fig. 7 6-MF activates HFrD-damaged autophagy via the AMPKα-mTOR pathway. Analysis of double-fluorescent mCherry-GFP-LC3B fusion protein expression to detect autophagic flux (yellow puncta represent autophagosomes and red puncta represent autolysosomes) in HepG2 cells under 15 μM 6-MF treatment with/without FA-fructose mixture (**a**). Fifty cells were used for the statistical analysis of the number of autophagosomes and autolysosomes per transfected cell (**b**) ($n = 5$). **c**, **d** Immunofluorescent staining for determination of autophagosomes (LC3B) and lipids (Nile red) in HepG2 cells under 15 μM 6-MF treatment with/without FA-fructose mixture ($n = 5$). **e**, **f** Protein expression levels of mTOR, pmTOR, AMPKα and pAMPKα in liver and HepG2 cells were determined by Western blot ($n = 3$). **g**, **h** In the condition of normal (lane 1–3) and compound C (10 μM, an AMPK inhibitor) treatment (lane 4–6), protein expression levels of mTOR, pmTOR, AMPKα, pAMPKα, CPT1α, Beclin1, P62 and LC3B in HepG2 cells were determined by Western blot ($n = 3$). All data are presented as the mean ± SEM, $^{*}P < 0.05$, $^{**}P < 0.01$, ns: not significant. For the quantitation of the band density, **e**, **f**: $^{*}P < 0.05$, $^{**}P < 0.01$ vs. NC-C/lane 1, $^{\#}P < 0.05$, $^{\#\#}P < 0.01$ vs. HFrD-C/lane 3; **g**, **h**: $^{*}P < 0.05$, $^{**}P < 0.01$ vs. lane 1, $^{\#}P < 0.05$, $^{\#\#}P < 0.01$ vs. lane 2, $^{\wedge}P < 0.05$, $^{\wedge\wedge}P < 0.01$ vs. lane 4.

C treatment (Fig. 7h, lane 5 vs. lane 6). We further investigated whether the regulation of the AMPKα-mTOR pathway by 6-MF is dependent on Nogo-B. We found that when Nogo-B was overexpressed, 6-MF failed to activate the AMPKα-mTOR pathway which was inhibited by the FA-fructose mixture. Ultimately, 6-MF can restore autophagic flux in damaged hepatocytes to promote lipolytic metabolism. This effect was achieved through the activation of the AMPKα-mTOR signaling pathway.

DISCUSSION

Unlike other isoforms of the Nogo family, Nogo-B is widely expressed across various tissues, including the liver, fat, muscle, and brain [15]. Nogo-B is not often expressed in hepatocytes. In contrast, it is barely expressed in normal hepatocytes, and its levels are increased in hepatocellular carcinoma cells or injured hepatocytes [11, 13]. Nogo-B plays an essential role in various liver diseases. Particularly, inhibition of Nogo-B expression is effective in preventing the development of metabolic diseases, indicating Nogo-B may be a possible therapeutic target for improving these metabolic diseases. At present, there are no effective inhibitors other than siRNA active on Nogo-B [12, 14, 15, 41]. Flavonoids are diverse, and many have pharmacological importance [42]. In this study, we selected 14 structurally simple and similar flavonoids for screening hepatocytes using a dual luciferase reporter system based on the Nogo-B transcriptional response system and identified the optimal inhibitor, 6-MF. 6-MF was able to significantly inhibit Nogo-B expression in vitro and in vivo while ameliorating high fructose-induced metabolic disorders and liver injury. Our study not only established an effective method for screening Nogo-B inhibitors but also assisted in the discovery of 6-MF, providing a new option and strategy for inhibiting Nogo-B expression.

Carbohydrates activate ChREBP to promote FFA synthesis. Excess FFA resulting from unlimited carbohydrate intake has lipotoxicity promoting the progression of NAFLD [43, 44]. Excess FFA accelerates liver damage by altering endoplasmic reticulum function, redox, autophagy, inflammatory response, and other mechanisms [38]. In this study, we determined that overexpression of Nogo-B antagonized lipid synthesis, oxidative stress, and inflammatory response which was inhibited by 6-MF (Fig. 5i-l). This suggests that the amelioration of liver injury by 6-MF is likely to be achieved through the inhibition of Nogo-B. As Nogo-B is involved in fructose-activated FFA synthesis via ChREBP [15], we hypothesized that 6-MF reduces ChREBP-mediated lipid synthesis through inhibition of Nogo-B, leading to a reduction in FFA level and reversal of liver injury. However, under ChREBP overexpression, 6-MF was still able to inhibit oxidative stress and inflammation (Fig. 6a–d), suggesting other mechanisms for 6-MF to ameliorate high-fructose-induced liver injury outside of the inhibition of FFA synthesis *via* the Nogo-B-ChREBP pathway.

Prolonged exposure of hepatocytes to FFA results in inhibition of autophagic flux and cell death [38]. An increasing number of studies indicate that the impairment of autophagic flux is associated with the development of NAFLD [45–47]. Autophagy is a catabolic process used to degrade cytoplasmic macromolecules (glycogen, proteins, lipids, and nucleic acids) during starvation or cellular stress. For example, lipid autophagy can catabolize TG into FFA and promote subsequent β-oxidation to maintain homeostasis of cellular metabolism [37]. Simultaneously, autophagy can selectively remove damaged mitochondria and excess lipid droplets, reducing steatosis and liver damage [37]. Based on the crucial role of lipid autophagy in liver injury, we examined mitochondrial oxidative phosphorylation, β-oxidation, and autophagic flux in hepatocytes and determined that these processes which were inhibited by high fructose were rescued by 6-MF treatment (Figs. 6e–h, 7a, b). Thus, our results suggested that, outside of inhibiting lipid synthesis, 6-MF reduced FFA accumulation through the restoration of autophagic flux and promoting β-oxidation of FFA.

In addition, mTOR, a central cell growth regulator responsible for regulating growth factors and trophic signals, is targeted to inhibit autophagy [48]. In contrast, the activation of AMPKα, a key energy sensor can inhibit mTOR activation and promote autophagy [49]. Several studies have indicated an important role for the AMPKα-mTOR pathway in autophagy [50, 51]. Our study demonstrated that 6-MF restored the autophagic flux damaged by high fructose via the AMPKα-mTOR pathway (Fig. 7c–f). However, AMPKα activation inhibits ChREBP-mediated fatty acid synthesis [52, 53]. SREBP1c, a transcription factor for the fatty acid synthesis genes FASN and ACC, whose nuclear translocation is inhibited by the activation of AMPKα [54, 55]. Thus, activation of AMPK enhances lipid autophagy while simultaneously inhibiting fatty acid synthesis. Inhibition of Nogo-B reduces ChREBP-mediated fatty acid synthesis independently of AMPKα [15], suggesting that 6-MF may inhibit fatty acid synthesis through inhibition of ChREBP and activation of AMPKα.

Surprisingly, Tian et al. [13] found that in normal hepatocellular carcinoma (HCC) cells, Nogo-B promotes the degradation of lipid droplets to provide energy for cancer cells, promoting cancer cell proliferation. While we used HCC cells for our in vitro experiments, we focused on the role of Nogo-B when hepatocytes undergo steatosis and damage. However, Nogo-B may function distinctly in pathological HCC cells compared to normal HCC cells. The role of Nogo-B in glucolipid metabolism is functionally opposite in normal and high glucose-stimulated HepG2 cells, as reported by Zhang et al. [15] In normal HepG2, the knockdown of Nogo-B activates ChREBP, while the knockdown of Nogo-B inhibits ChREBP under high glucose stimulation conditions.

Ultimately, our study identifies and demonstrates for the first time that 6-MF can effectively inhibit Nogo-B expression in the liver, providing a new approach and option for the development of Nogo-B inhibitors. Simultaneously, 6-MF improves FFA accumulation through the restoration of autophagic flux and also suggests a new potential mechanism by which Nogo-B deficiency inhibits hepatic metabolic diseases, requiring further focus and study.

ACKNOWLEDGEMENTS

Support was provided by China NSFC grants U22A20272 and 82173807 to YJD, 81973316 to JHH; Tianjin Municipal Science and Technology Commission of China Grant 20JCZDJC00710 and the Fundamental Research Funds for the Central Universities (Nankai University) 63211045 to JHH.

AUTHOR CONTRIBUTIONS

KG, ZZ, QSL, JHH, and YJD designed the study, drafted and edited the manuscript; KG and ZZ performed most of the experiments; SSC, XRZ, MYW, XYY, and CD assisted with the experimental operation or data collection.

ADDITIONAL INFORMATION

Supplementary information The online version contains supplementary material available at https://doi.org/10.1038/s41401-023-01121-7.

Competing interests: The authors declare no competing interests.

REFERENCES

1. Bray GA, Nielsen SJ, Popkin BM. Consumption of high-fructose corn syrup in beverages may play a role in the epidemic of obesity. Am J Clin Nutr. 2004;79:537–43.
2. Malik VS, Popkin BM, Bray GA, Despres JP, Hu FB. Sugar-sweetened beverages, obesity, type 2 diabetes mellitus, and cardiovascular disease risk. Circulation. 2010;121:1356–64.
3. Johnson RJ, Sanchez-Lozada LG, Andrews P, Lanaspa MA. Perspective: a historical and scientific perspective of sugar and its relation with obesity and diabetes. Adv Nutr. 2017;8:412–22.
4. Hannou SA, Haslam DE, McKeown NM, Herman MA. Fructose metabolism and metabolic disease. J Clin Invest. 2018;128:545–55.
5. Diggle CP, Shires M, Leitch D, Brooke D, Carr IM, Markham AF, et al. Ketohexokinase: expression and localization of the principal fructose-metabolizing enzyme. J Histochem Cytochem. 2009;57:763–74.
6. Kim MS, Krawczyk SA, Doridot L, Fowler AJ, Wang JX, Trauger SA, et al. ChREBP regulates fructose-induced glucose production independently of insulin signaling. J Clin Invest. 2016;126:4372–86.
7. Federico A, Rosato V, Masarone M, Torre P, Dallio M, Romeo M, et al. The role of fructose in non-alcoholic steatohepatitis: old relationship and new insights. Nutrients. 2021;13:1314.

8. Oertle T, Huber C, van der Putten H, Schwab ME. Genomic structure and functional characterisation of the promoters of human and mouse nogo/rtn4. J Mol Biol. 2003;325:299–323.
9. Di Lorenzo A, Manes TD, Davalos A, Wright PL, Sessa WC. Endothelial reticulon-4B (Nogo-B) regulates ICAM-1-mediated leukocyte transmigration and acute inflammation. Blood. 2011;117:2284–95.
10. Zhang D, Utsumi T, Huang HC, Gao L, Sangwung P, Chung C, et al. Reticulon 4B (Nogo-B) is a novel regulator of hepatic fibrosis. Hepatology. 2011;53:1306–15.
11. Gao L, Utsumi T, Tashiro K, Liu B, Zhang D, Swenson ES, et al. Reticulon 4B (Nogo-B) facilitates hepatocyte proliferation and liver regeneration in mice. Hepatology. 2013;57:1992–2003.
12. Park JK, Shao M, Kim MY, Baik SK, Cho MY, Utsumi T, et al. An endoplasmic reticulum protein, Nogo-B, facilitates alcoholic liver disease through regulation of kupffer cell polarization. Hepatology. 2017;65:1720–34.
13. Tian Y, Yang B, Qiu W, Hao Y, Zhang Z, Yang B, et al. ER-residential Nogo-B accelerates NAFLD-associated HCC mediated by metabolic reprogramming of oxLDL lipophagy. Nat Commun. 2019;10:3391.
14. Zhang S, Yu M, Guo F, Yang X, Chen Y, Ma C, et al. Rosiglitazone alleviates intrahepatic cholestasis induced by alpha-naphthylisothiocyanate in mice: the role of circulating 15-deoxy-Delta(12,14) -PGJ2 and Nogo. Br J Pharmacol. 2020;177:1041–60.
15. Zhang S, Guo F, Yu M, Yang X, Yao Z, Li Q, et al. Reduced Nogo expression inhibits diet-induced metabolic disorders by regulating ChREBP and insulin activity. J Hepatol. 2020;73:1482–95.
16. Chalasani N, Younossi Z, Lavine JE, Charlton M, Cusi K, Rinella M, et al. The diagnosis and management of nonalcoholic fatty liver disease: practice guidance from the American Association for the Study of Liver Diseases. Hepatology. 2018;67:328–57.
17. Chen Q, Wang T, Li J, Wang S, Qiu F, Yu H, et al. Effects of natural products on fructose-induced nonalcoholic fatty liver disease (NAFLD). Nutrients. 2017;9:96.
18. Hostetler GL, Ralston RA, Schwartz SJ. Flavones: food sources, bioavailability, metabolism, and bioactivity. Adv Nutr. 2017;8:423–35.
19. Swapna Sasi US, Sindhu G, Raghu KG. Fructose-palmitate based high calorie induce steatosis in HepG2 cells via mitochondrial dysfunction: an in vitro approach. Toxicol Vitr. 2020;68:104952.
20. Zhao L, Guo X, Wang O, Zhang H, Wang Y, Zhou F, et al. Fructose and glucose combined with free fatty acids induce metabolic disorders in HepG2 cell: a new model to study the impacts of high-fructose/sucrose and high-fat diets in vitro. Mol Nutr Food Res. 2016;60:909–21.
21. Maher P, Salgado KF, Zivin JA, Lapchak PA. A novel approach to screening for new neuroprotective compounds for the treatment of stroke. Brain Res. 2007;1173:117–25.
22. Gutierrez-Venegas G, Bando-Campos CG. The flavonoids luteolin and quercetagetin inhibit lipoteichoic acid actions on H9c2 cardiomyocytes. Int Immunopharmacol. 2010;10:1003–9.
23. Yu M, Zhang S, Guo F, Yang X, Li Q, Wei Z, et al. Identification of Nogo-B as a new molecular target of peroxisome proliferator-activated receptor gamma. Cell Signal. 2020;65:109429.
24. Clarkson AN, Boothman-Burrell L, Dosa Z, Nagaraja RY, Jin L, Parker K, et al. The flavonoid, 2′-methoxy-6-methylflavone, affords neuroprotection following focal cerebral ischaemia. J Cereb Blood Flow Metab. 2019;39:1266–82.
25. Shukla S, Gupta S. Molecular targets for apigenin-induced cell cycle arrest and apoptosis in prostate cancer cell xenograft. Mol Cancer Ther. 2006;5:843–52.
26. Chen Y, Duan Y, Yang X, Sun L, Liu M, Wang Q, et al. Inhibition of ERK1/2 and activation of LXR synergistically reduce atherosclerotic lesions in ApoE-deficient mice. Arterioscler Thromb Vasc Biol. 2015;35:948–59.
27. Duan Y, Chen Y, Hu W, Li X, Yang X, Zhou X, et al. Peroxisome proliferator-activated receptor gamma activation by ligands and dephosphorylation induces proprotein convertase subtilisin kexin type 9 and low density lipoprotein receptor expression. J Biol Chem. 2012;287:23667–77.
28. Wen H, Zhong Y, Yin Y, Qin K, Yang L, Li D, et al. A marine-derived small molecule induces immunogenic cell death against triple-negative breast cancer through ER stress-CHOP pathway. Int J Biol Sci. 2022;18:2898–913.
29. Liu Y, Wei Z, Ma X, Yang X, Chen Y, Sun L, et al. 25-Hydroxycholesterol activates the expression of cholesterol 25-hydroxylase in an LXR-dependent mechanism. J Lipid Res. 2018;59:439–51.
30. Xu K, Yang Y, Feng GH, Sun BF, Chen JQ, Li YF, et al. Mettl3-mediated m(6)A regulates spermatogonial differentiation and meiosis initiation. Cell Res. 2017;27:1100–14.
31. Jegatheesan P, De Bandt JP. Fructose and NAFLD: the multifaceted aspects of fructose metabolism. Nutrients. 2017;9:230.
32. Jegatheesan P, Beutheu S, Ventura G, Nubret E, Sarfati G, Bergheim I, et al. Citrulline and nonessential amino acids prevent fructose-induced nonalcoholic fatty liver disease in rats. J Nutr. 2015;145:2273–9.
33. Zambo V, Simon-Szabo L, Szelenyi P, Kereszturi E, Banhegyi G, Csala M. Lipotoxicity in the liver. World J Hepatol. 2013;5:550–7.
34. Zhang D, Tong X, VanDommelen K, Gupta N, Stamper K, Brady GF, et al. Lipogenic transcription factor ChREBP mediates fructose-induced metabolic adaptations to prevent hepatotoxicity. J Clin Invest. 2017;127:2855–67.
35. Mota M, Banini BA, Cazanave SC, Sanyal AJ. Molecular mechanisms of lipotoxicity and glucotoxicity in nonalcoholic fatty liver disease. Metabolism. 2016;65:1049–61.
36. Byrnes K, Blessinger S, Bailey NT, Scaife R, Liu G, Khambu B. Therapeutic regulation of autophagy in hepatic metabolism. Acta Pharm Sin B. 2022;12:33–49.
37. Cursio R, Colosetti P, Codogno P, Cuervo AM, Shen HM. The role of autophagy in liver diseases: mechanisms and potential therapeutic targets. Biomed Res Int. 2015;2015:480508.
38. Rada P, Gonzalez-Rodriguez A, Garcia-Monzon C, Valverde AM. Understanding lipotoxicity in NAFLD pathogenesis: is CD36 a key driver? Cell Death Dis. 2020;11:802.
39. Levine B, Kroemer G. Biological functions of autophagy genes: a disease perspective. Cell. 2019;176:11–42.
40. Gao Y, Fan X, Gu W, Ci X, Peng L. Hyperoside relieves particulate matter-induced lung injury by inhibiting AMPK/mTOR-mediated autophagy deregulation. Pharmacol Res. 2021;167:105561.
41. Wang X, Yang Y, Zhao D, Zhang S, Chen Y, Chen Y, et al. Inhibition of high-fat diet-induced obesity via reduction of ER-resident protein Nogo occurs through multiple mechanisms. J Biol Chem. 2022;298:101561.
42. Cao Y, Xie L, Liu K, Liang Y, Dai X, Wang X, et al. The antihypertensive potential of flavonoids from Chinese Herbal Medicine: a review. Pharmacol Res. 2021;174:105919.
43. Benhamed F, Denechaud PD, Lemoine M, Robichon C, Moldes M, Bertrand-Michel J, et al. The lipogenic transcription factor ChREBP dissociates hepatic steatosis from insulin resistance in mice and humans. J Clin Invest. 2012;122:2176–94.
44. Gambino R, Bugianesi E, Rosso C, Mezzabotta L, Pinach S, Alemanno N, et al. Different serum free fatty acid profiles in NAFLD subjects and healthy controls after oral fat load. Int J Mol Sci. 2016;17:479.
45. Gonzalez-Rodriguez A, Mayoral R, Agra N, Valdecantos MP, Pardo V, Miquilena-Colina ME, et al. Impaired autophagic flux is associated with increased endoplasmic reticulum stress during the development of NAFLD. Cell Death Dis. 2014;5:e1179.
46. Amorim R, Simoes ICM, Teixeira J, Cagide F, Potes Y, Soares P, et al. Mitochondria-targeted anti-oxidant AntiOxCIN4 improved liver steatosis in Western diet-fed mice by preventing lipid accumulation due to upregulation of fatty acid oxidation, quality control mechanism and antioxidant defense systems. Redox Biol. 2022;55:102400.
47. Zhou J, Tripathi M, Ho JP, Widjaja AA, Shekeran SG, Camat MD, et al. Thyroid hormone decreases hepatic steatosis, inflammation, and fibrosis in a dietary mouse model of nonalcoholic steatohepatitis. Thyroid. 2022;32:725–38.
48. Kim YC, Guan KL. mTOR: a pharmacologic target for autophagy regulation. J Clin Invest. 2015;125:25–32.
49. Egan D, Kim J, Shaw RJ, Guan KL. The autophagy initiating kinase ULK1 is regulated via opposing phosphorylation by AMPK and mTOR. Autophagy. 2011;7:643–4.
50. Sun D, Tao W, Zhang F, Shen W, Tan J, Li L, et al. Trifolirhizin induces autophagy-dependent apoptosis in colon cancer via AMPK/mTOR signaling. Signal Transduct Target Ther. 2020;5:174.
51. Jia J, Abudu YP, Claude-Taupin A, Gu Y, Kumar S, Choi SW, et al. Galectins control MTOR and AMPK in response to lysosomal damage to induce autophagy. Autophagy. 2019;15:169–71.
52. Zhang Y, Li C, Li X, Wu C, Zhou H, Lu S, et al. Trimetazidine improves hepatic lipogenesis and steatosis in non-alcoholic fatty liver disease via AMPK-ChREBP pathway. Mol Med Rep. 2020;22:2174–82.
53. Balamurugan K, Medishetti R, Kotha J, Behera P, Chandra K, Mavuduru VA, et al. PHLPP1 promotes neutral lipid accumulation through AMPK/ChREBP-dependent lipid uptake and fatty acid synthesis pathways. iScience. 2022;25:103766.
54. Han Y, Hu Z, Cui A, Liu Z, Ma F, Xue Y, et al. Post-translational regulation of lipogenesis via AMPK-dependent phosphorylation of insulin-induced gene. Nat Commun. 2019;10:623.
55. Herzig S, Shaw RJ. AMPK: guardian of metabolism and mitochondrial homeostasis. Nat Rev Mol Cell Biol. 2018;19:121–35.